Environmental Earth Sciences (2024) 83:354
https://doi.org/10.1007/s12665-024-11671-6

ORIGINAL ARTICLE

Analysis of heavy precipitation-induced rill erosion

Rebecca Hinsberger[1,2]

Received: 29 December 2023 / Accepted: 11 May 2024 / Published online: 22 May 2024

Abstract
Erosion is an ongoing environmental problem that leads to soil loss and damages ecosystems downstream of agriculture. Increasingly frequent heavy precipitation causes single erosion events with potentially high erosion rates owing to gully erosion. In this study, analyses of croplands affected by heavy precipitation and linear erosion indicate that erosion occurs only on sparsely vegetated fields with land cover $\leq 25\%$ and that slope gradient and length are significant factors for the occurrence of linear erosion tracks. Existing erosion models are not calibrated to the conditions of heavy precipitation and linear erosion, namely high precipitation intensities and long and steep croplands. In this study, natural linear erosion was analyzed using an unmanned aerial vehicle and erosion volumes were determined for 32 rills and gullies of different sizes. Comparisons with the RUSLE2 and EROSION-3D model values showed an underestimation of linear erosion in both models. Therefore, calibration data for erosion models used for heavy precipitation conditions must be adapted. The data obtained in this study meet the required criteria.

Keywords Rill erosion · Gully erosion · Flash flood · UAV · RUSLE2 · EROSION-3D (E3D)

Introduction

Terrestrial ecosystems and especially soils are the fundamental basis for life on earth and are a resource for high-priority protection. However, the continuous increase in the world population has led to the intensified use of soil for arable land and, consequently, competition for use between food, fodder, and energy production or nature preservation. The process that damages soil is erosion. The Intergovernmental Panel on Climate Change (IPCC) Special Report (2021) indicated that erosion is a significant factor in land degradation and desertification. In this study, water-induced soil erosion in conjunction with heavy precipitation was investigated.

Previously, erosion models were developed to forecast soil losses. Existing soil erosion models can be divided into empirical, conceptual, and process-oriented or physically based models, developed for different central issues, depending on the nature and characteristics of the model and the intended application (Andualem et al. 2023). Models such as the well-known Universal Soil Loss Equation (USLE) (Wischmeier and Smith 1978) are useful for simulating long-term erosion, whereas the Water Erosion Prediction Project (WEPP) (Laflen et al. 1991) and the European Soil Erosion Model (EUROSEM) (Morgan et al. 1998) are suitable for single events. Simple empirical models, such as the USLE, have a small number of input parameters that are relatively easy to obtain. This contrasts with models such as EUROSEM, which are based on a large amount of input information. However, data acquisition is difficult. Detailed lists of existing erosion models for different aims have been provided in review articles (e.g., Andualem et al. 2023; Borelli et al. 2021; Michael 2000).

Thus far, many of the existing erosion models have been based on experimental studies to calculate the erosion quantity. Two main types of erosion can be distinguished: sheet and linear erosion. Sheet erosion occurs over the entire surface of arable land, where the soil is evenly eroded as thin sheets. Linear erosion is characterized by linear shapes, such as grooves (rills) or deeper and wider gullies. These shapes are formed by the friction of water in the resulting flow paths. To detect sheet erosion, time series were observed

✉ Rebecca Hinsberger
rebecca.hinsberger@uni-saarland.de

[1] Physical Geography and Environmental Research, Saarland University, 66123 Saarbrücken, Germany

[2] Hydraulic Engineering and Water Management, School of Architecture and Civil Engineering, University of Applied Sciences, 66117 Saarbrücken, Germany

by Cândido et al. (2020) and Pineux et al. (2017), whereas Eltner et al. (2015) and Kou et al. (2020) recorded multi-temporal soil surface changes. Linear erosion can be identified visually (as opposed to sheet erosion) and has been investigated using different indirect methods, such as specifically designed kites (Giménez et al. 2009), fixed-wing aircraft (D'Oleire-Oltmanns et al. 2012; Peter et al. 2014), and quadrocopters (Di Stefano et al. 2019). Some studies have conducted laboratory erosion experiments at the plot scale (Aksoy et al. 2013; Di Stefano et al. 2017; Tackmann 2010), whereas others have conducted field investigations (Bruno et al. 2008; Carollo et al. 2015; Wirtz et al. 2010, 2012). Furthermore, studies have investigated the erosion caused by natural rainfall (Bruno et al. 2008; Carollo et al. 2015), rainfall simulators (Aksoy et al. 2013; Polyakov et al. 2018; Römkens et al. 2001; Zhang et al. 2021), and overland flow (Di Stefano et al. 2017). In addition to the mere recording of erosion, post-processing the detection of erosion shapes and assessing erosion volumes are important steps in producing useful data for erosion model calibration and validation. In terms of detecting the spatial extent of erosion rills, Malinowski et al. (2022) developed an automatic recognition and mapping of erosion rills at the field scale. In terms of volumetric assessments, previous studies have dealt with the reconstruction of the original surface (pre-erosion). D'Oleire-Oltmanns et al. (2012) and Peter et al. (2014) derived a 3D polygon from rill edges, whereas Báčová et al. (2019) presented an algorithm and Python implementation for automatic volume calculations in a geo-information system (GIS). In recent decades, several studies have focused on the continuous development and forecasting of erosion (Boardman and Favis-Mortlock 1998; Borelli et al. 2021; Bryan 1990; Morgan and Nearing 2011).

However, a large portion of the total eroded material is affected by a few heavy precipitation events (Parkin et al. 2008), causing damage also downstream the eroded field. These extreme events are expected to increase in frequency and intensity owing to climate change (IPCC 2021). Heavy precipitation often leads to linear erosion, such as rills and gullies. Several studies have investigated the quantity and spread of erosion and sedimentation in test plots using rainfall simulators (Aksoy et al. 2013; Polyakov et al. 2018; Römkens et al. 2001; Zhang et al. 2021). However, laboratory and in-situ test plots are often limited in size. Linear erosion requires space to develop from precipitation-induced overland flow. The decision for model usability is based on the data used for calibrating the erosion quantity (Malinowski et al. 2022; Pineux et al. 2017). Data for the USLE model contains test plots in various sizes, slopes and cropping which are compared with the unit plot that is 22.1 m in length, 1.87 m in width, and has a 9% gradient (Carollo et al. 2024; Schwertmann et al. 1987; Wischmeier and Smith 1978). In the EROSION-3D (E3D) model, the test plots were 0.64×0.24 m for experiments to derive the erosion quantity (Schmidt 1984, 1988) and 22 m long and 2 m or 4 m wide (USLE unit plots) for experiments to derive erosion resistance and correction factors (Michael et al. 1996; Michael 2000). Besides including linear erosion conditions, the precipitation and discharge that leads to specific erosion forms are important factors. In existing calibration data, precipitation intensity often does not correspond to heavy precipitation events [intensity ≥ 15 mm/h (DWA n.d.)] or are sometimes neglected in erosion meta data. Investigations of the USLE, for example, include various events in different years (Schwertmann et al. 1987; Wischmeier and Smith 1978), whereas E3D uses erosion quantities based on experiments with rainfall simulators with intensities up to 54 mm/h (Michael 2000; Schmidt 1988).

This study focused on linear erosion based on single heavy precipitation events at the hillslope scale. For croplands affected by heavy precipitation, framework conditions were analyzed to determine the significant factors for the occurrence of linear erosion. When linear erosion occurred, the surface structures were collected at the hillslope scale using an unmanned aerial vehicle (UAV) and manual field measurements, and the erosion volumes of the rills were quantified. The erosion quantities of these natural events were determined and compared with results obtained using existing erosion models. As the data requirement for the USLE family models is affordable and the models are one of the most commonly used erosion models (Borelli et al. 2021), the RUSLE2 model that is applicable for single days was used for comparison. In addition, E3D was selected for comparison because of the possibility of simulating single precipitation events and erosion quantity data based on heavy precipitation intensity.

Materials and methods

Measurements of eroded croplands are important for addressing the overarching objective of using erosion quantities from natural events for model calibration. To achieve this objective, several steps are necessary: (a) localization of erosion due to local heavy precipitation events, (b) on-site recording of erosion, (c) photogrammetric analysis of erosion to generate a digital elevation model (DEM) of arable land, and (d) analysis of the DEM as a basis for quantifying erosion and delineating the spatial distribution of erosion tracks. For three years, heavy precipitation events that occurred in Saarland, Germany (federal state with 2500 km^2) and neighboring states, were investigated with respect to the occurrence and extent of erosion.

Localization of erosion

The measurement of erosion due to natural precipitation (compared with rainfall simulators) requires the localization of heavy precipitation events. The German Meteorological Service (Deutscher Wetterdienst, DWD) defines precipitation as having at least 15 mm/h intensity as heavy precipitation. A challenge in this localization is the local limitation and occurrence of extreme events. One method of delimiting potential areas is to use radar data. The RY-RADOLAN data from the DWD show precipitation intensities and have a temporal resolution of 5 min and a spatial resolution of 1 km^2 (DWD 2004, 2017). These data are provided online shortly after their occurrence. To display precipitation intensities, the Flood Early Warning System (FEWS) software (Deltares, Delft, The Netherlands) (Deltares n.d.) was used in this study. The areas affected by heavy precipitation were categorized based on land usage. A pre-selection of areas that are agriculturally used and affected by heavy precipitation has thus already been made. All these arable land areas were inspected on-site for erosion one to two days after the event. The croplands were identified and visually inspected for signs of erosion (gullies, rills, sedimentation tracks). A total of 456 croplands affected by heavy precipitation were examined for erosion. For these fields, framework conditions (erosion type, land cover, amount of precipitation, slope length and gradient) were collected on-site and/or by analyzed geodata.

Linear erosion measurements

When linear erosion occurred, the cropland areas were recorded using a UAV. The approach of using UAVs for erosion recording was suggested by the German Association for Water, Wastewater, and Waste (DWA) (DWA 2020) and has been performed in previous studies (see Introduction). In this study, croplands with linear erosion were investigated using the DJI Phantom 4 RTK (real-time kinematic) (P4RTK) UAV. Preliminary tests were conducted using the UAV to investigate accuracy. Comparisons of P4RTK with manual measurements using a measuring stick at linear erosion tracks show good correspondence for the rill width, with an Root Mean Square Error (RMSE) of 10.7 cm for rills that were up to 350 cm wide. For the rill depth, the erosion tracks in the UAV measurements were underestimated. Here, the RMSE was 2.11 cm for rills up to 20 cm. For the following study, errors in this range of values must be considered.

Aerial surveys were conducted one or two days after heavy precipitation events at the hillslope scale. Photographs taken by the UAV were aligned, and a dense point cloud was built before generating a DEM (hereinafter referred to as rill DEM) and an orthoimage with the structure from motion technique using the Agisoft Metashape Professional software (Agisoft LLC, St. Petersburg, Russia) (Agisoft LLC n.d.). All UAV- and event-related information is listed in Table 1.

In addition, two undisturbed soil samples were taken in from each field at the day of the aerial survey using predefined cylinders. These soil samples were examined in laboratory tests in accordance with DIN 18125–2 (2020) to determine the bulk density of the croplands. Besides, a few months after the event, 5 disturbed soil samples per field were taken from the upper soil layer (0–20 cm). These samples were analyzed regarding particle size distribution using sieve and sedimentation analyses (DIN EN ISO 17892-4:2017-04 2017b). The soil types were derived from these results.

Analysis of erosion quantity

By recording the surface of fields affected by erosion, high-quality data were available for reporting the conditions after the erosion event. However, heavy precipitation occurs in limited areas and has short forecasting times. Consequently, prior measurements of the erosion areas and data on the situation before an erosion event are usually not available due to the research approach. A pre-erosion dataset similar to the original surface must be available to calculate the groove width, depth, and erosion quantity. One possible dataset is a DEM with a spatial resolution of 1×1 m, which is available from regional authorities. However, the accuracy of ± 20 cm, stated by the regional authority (LVGL 2019), is higher than most of the recorded rill depths, and the resolution of 1 m is much higher than most of the recorded rill widths. Another possibility is to create a pre-erosion dataset from the recorded high-resolution rill DEM data. In this study, a pre-erosion dataset was created using the volumetric loss measurement technique, which is a modified approach proposed by Peter et al. (2014). Erosion tracks were identified using the following steps. The rill DEM was converted to a mesh, which was modified with the Surface-water Modeling System (SMS) (Aquaveo LLC, Provo, UT, United States) (Aquaveo n.d.). In this mesh, all points in the erosion area were deleted to generate a surface unaffected by erosion. The orthoimage and superelevation of the mesh helped identify the affected and unaffected field parts. Thereafter, the gap in the mesh was retriangulated with the SMS workflow "mesh node triangulation." In this workflow, triangular elements were generated between the boundary nodes (Aquaveo n.d.). Subsequently, the mesh was converted into a raster. The final product was a DEM with smoothed erosion areas, called a pre-erosion DEM. Figure 1a shows an example of a rill area in Field 6. Figure 1b and c show one rill in the rill DEM and smoothed pre-erosion DEM, respectively. The differences between the rill and pre-erosion DEM were determined using a raster calculator (DEMs of difference). This process

Table 1 Information on investigated areas and flight metrics for Fields 1–9

Field	UAV mode	DEM extent [ha]	Flight date	Flight height [m]	Number of pictures	Overlapping [%]		Speed [m/s]	Obtained resolution [cm/px]	Precipitation intensity [mm/h]	Geographical position (Lon/Lat)
						Horizontal	Vertical				
1	2D	8.29	21 May, 2022	40	497	70	80	3.1	2.7	51.81	7.287492 /49.235052
2	2D	8.24	23 June, 2021	50	230	70	80	3.9	3.2	19.1	7.251585 /49.201051
3	2D	9.94	20 May, 2022	40	552	70	80	3.1	2.0	14.42 + 19.43	7.196362 /49.517098
4	2D	7.37	20 May, 2022	40	312	70	80	3.1	3.0	11.60 + 19.37	6.976104 /49.443117
5	2D	7.37	20 May, 2022	40	312	70	80	3.1	3.0	11.60 + 19.37	6.976587 /49.442301
6	2D	2.58	21 May, 2022	40	120	70	80	3.1	2.0	53.05	7.342572 /49.270588
7	2D	13.75	21 May, 2022	40	557	70	80	3.1	3.5	66.92	7.339650 /49.267832
8	2D	37.30	05 June, 2021	70	449	70	80	4.5	4.1	46.19	6.757593 /49.527604
9	2D	37.30	05 June, 2021	70	449	70	80	4.5	4.1	46.19	6.758614 /49.525492
10	2D	14.07	23 May, 2023	50	614	70	80	3.9	2.8	28.59	6.846149 /49.553545
11	2D	32.91	18 May, 2023	50	1,014	70	80	3.9	4.9	23.82	6.981664 /49.390056

provided the groove depth at each grid point. Positive and negative values distinguished between erosion and sedimentation. The product of the erosion depth and raster resolution was the erosion volume.

A limitation of this approach is the assumption that the recorded heavy precipitation event is the only event that led to erosion between sowing and the UAV survey.

Erosion models

For the comparison of the calculated natural erosion data of this study with existing models, the detachment share of the empirical model RUSLE2 was used as well as the more physically based model E3D (GeoGnostics, Berlin, Germany) (GeoGnostics n.d.).

The RUSLE2 calculates the rill and interrill (sheet) erosion based on five basic factors of the USLE that are assumed for the day of the event: rainfall erosivity factor *R*, soil erodibility factor *K*, topographic factors (slope gradient *S* and length *L*), crop cover and management factor *C*, and protection factor *P* (Wischmeier and Smith 1978). In this study, rainfall erosivity factor R was derived from YW-RADKLIM radar data provided by the German Meteorological Service (DWD) for a specific event (Winterrath et al. 2018). These data have spatial and temporal resolutions of 1×1 km^2 and 5 min, respectively and show quasi gauge-adjusted five-minute precipitation rates in Germany. For the calculation of the RUSLE2, the R factor was calculated using the EI30 index, the product of the kinetic energy, E, and the maximum precipitation intensity over 30 min, I30 (DIN 19708 2017a). Here, E is the sum of all periods with a constant intensity. The soil erodibility (K factor) was derived from the soil type. The soil types of the soil samples taken in this study, were compared with the soil types of a soil map [scale: 1:5000 (LVGL n.d.)]. The derived K factors were the same for 50% of the samples and differed by 0.05 for the other half of the soil samples. As soil analyses were not carried out for all fields, the soil type from the map was used to derive the K factor for reasons of comparability. Both the R and K factors are calculated according to the equations of DIN 19708 (2017a), as these are suitable for German conditions. The L and S factor were calculated according to the User's Reference Guide of the RUSLE2 (USDA 2008). Here, the ratio of rill and interrill erosion β was considered by using the slope and land cover that were determined and analyzed in the Localization of erosion section. The ration of rill and interrill erodibility Kr/Ki and the rill to interrill ration for prior land use cpr/cpi were derived from the science documentation of the RUSLE2 (USDA 2013). As not all information were available for the latter parameters, worst case parameters were used. As the fields show, in general,

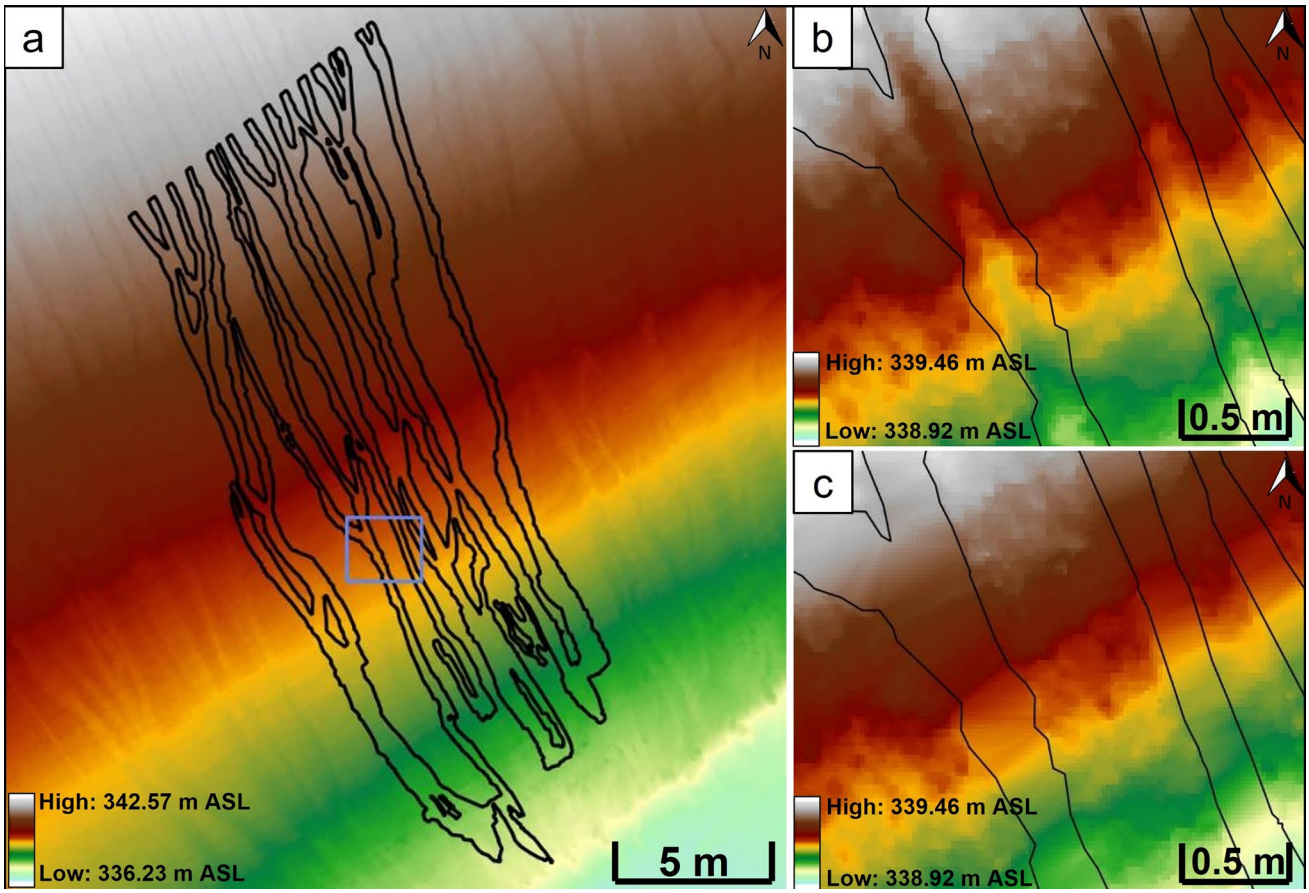

Fig. 1 Example of the triangulation method used to create the pre-erosion surface. **a** Perimeter of Field 6, erosion area 2; details of **b** erosion area in the recorded rill DEM, and **c** pre-erosion surface with closed erosion area, obtained using the mesh node triangulation method

a uniform topography, a differentiated analysis of hillslope segments was not carried out. The C factor is considered as 1-covering factor and the P factor was neglected.

For the comparison with the natural erosion data of this study, only the rill share of the RUSLE2 was considered. The amount of RUSLE 2 rill erosion is calculated as difference between the results of RUSLE2 equation for rill and interrill erosion (described above) and the corresponding interrill erosion only. The interrill erosion is calculated according to the science documentation of the RUSLE2 (USDA 2013, Eq. 2.11).

For the simulation using E3D, the precipitation load was taken into account by the time series of the precipitation intensity based on the YW data of the DWD. The soil characteristics were derived from the soil type using the guideline by Michael et al. (1996). In the model, various parameter, such as the critical momentum flux, are derived from the soil input information. The topography was considered by the DEM. As the minimum resolution for the input data was 1×1 m, the DEM available from the regional authorities was used.

Results and discussion

All croplands investigated in this study were analyzed to determine the factors that are most important for the occurrence of linear erosion tracks due to heavy precipitation. For fields where linear erosion was detected, the erosion volume was quantified and then compared with the results of the RUSLE2 and E3D model applications. For fields where no linear erosion or sedimentation tracks could be detected, the amount of erosion was considered irrelevant.

Influencing factors of erosion

In this study, 456 croplands were investigated after different heavy precipitation events. All fields vary in their locations and, consequently, in their framework conditions (e.g., slope length, gradient, or land cover). Among these fields, 141 were not covered or were covered very little,

and 315 were fully covered with different agricultural crops, for example, different types of grain or grassland. Of these 141 bare-soil fields, visible linear and/or sheet erosion occurred in 20 (see Sect. Localization of erosion). As a result, erosion occurred only in vegetation-free, sparsely covered fields. In one vegetation-covered field, only small erosion tracks from previous events (overgrown rills) were detected.

For all fields, framework conditions such as slope length, gradient, land cover, and precipitation were analyzed. However, not all data were available for one event. Therefore, 30 fields were excluded and 426 fields were used for subsequent analyses. All fields were classified according to the erosion type to determine which factors were relevant and when erosion started. The fields were divided into "linear erosion with partly occurring sheet erosion" (n = 15), "exclusively sheet erosion" (n = 5), and "no erosion" (n = 406). Figure 2 shows four box plots, including the influence of different factors on erosion types.

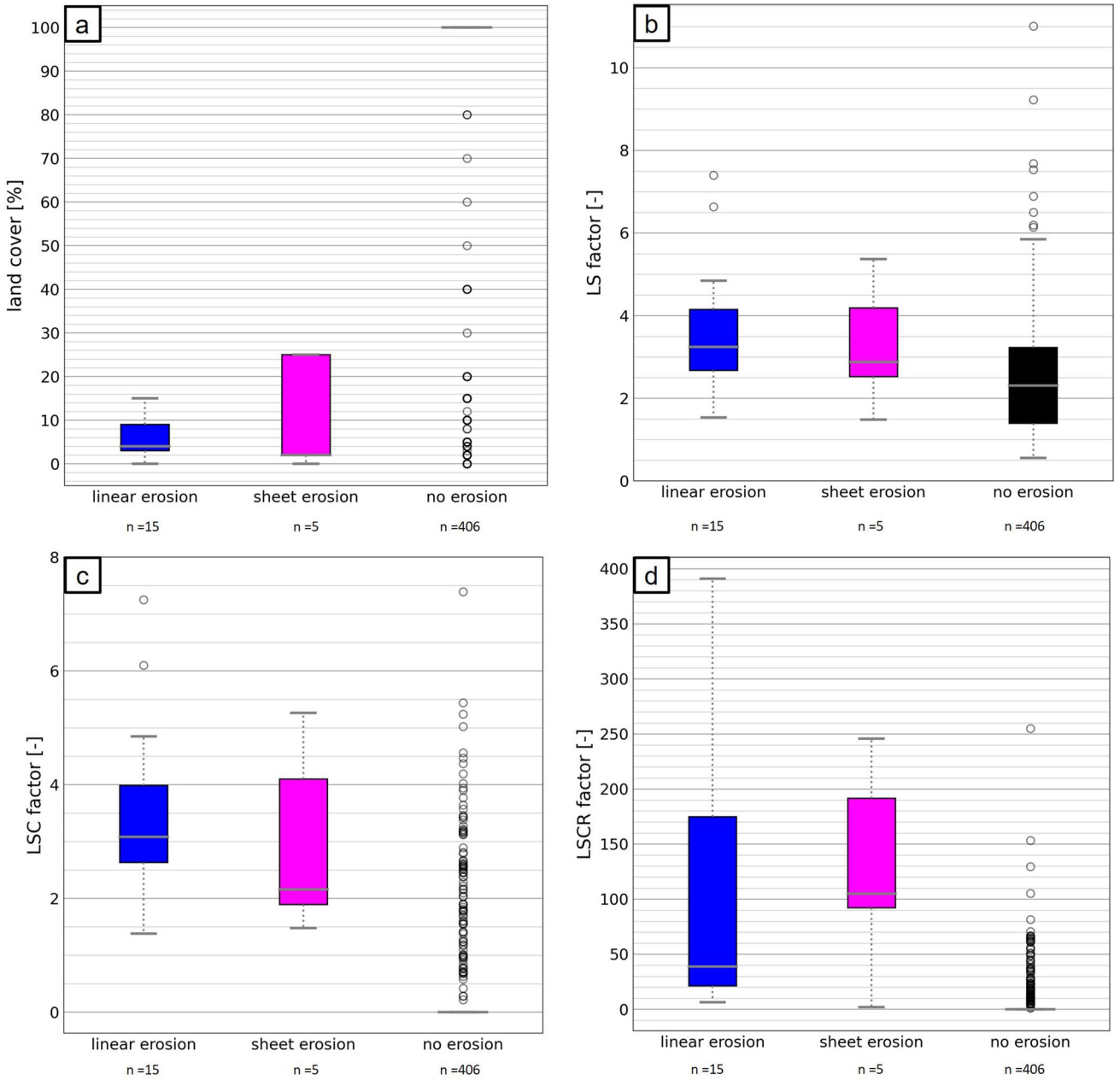

Fig. 2 Comparison of **a** share of land cover, **b** LS factor, **c** LSC factor, and **d** LSCR factor influencing linear erosion, sheet erosion, and no erosion fields. The boxplots display the interquartile range (boxes), the median (horizontal gray lines), the 25th and 75th percentiles (horizontal gray lines), and outliers (circles)

A comparison of the erosion types with respect to *land cover* (Fig. 2a) showed that linear and/or sheet erosion occurred only in sparsely covered fields. No erosion could be detected on fields with a cover ≥ 25%. This threshold corresponds to values reported by Armand et al. (2009). They stated that land cover > 30% reduces soil crusting and, consequently, overland flow as well as erosion. For the 406 fields that were assigned to the "no erosion" group, 75% showed a land cover of 100% and 25% did not show full cover. For these 25%, other impact factors were the decisive as to why no erosion had taken place. The analysis of the *LS factor* (Fig. 2b) indicated small differences for all erosion types. The interquartile range was lower for the "no erosion" type than the range for linear and sheet erosion. However, the overall span and number of outliers were higher for fields with no erosion. This result indicates an even distribution of the LS factor for all 426 investigated fields. By aggregating LS and land cover, land cover was transferred to the C factor by considering the share of uncovered soil (1 − land cover). As the land cover for "no erosion" fields tended to 100%, the *LSC factor* for this group was very low (Fig. 2c). Considering the precipitation with the R factor, the linear and sheet erosion fields showed a high value range (Fig. 2d). For "no erosion" type fields, there was still a high number of outliers with values as high as those of the linear and sheet erosion fields. However, values that seemed very high for the "no erosion" category can be explained by one dominant factor, e.g., very high precipitation intensity or a very high slope gradient. All the factors influenced the different erosion categories. Land cover, in particular, exerted a strong influence on the "no erosion" fields. No difference was apparent between linear and sheet erosion.

Analysis of erosion quantity

Of the 426 investigated croplands, 15 fields exhibited linear erosion tracks with different rill and gully types. Some fields showed many small rills (a few centimeters wide and deep), whereas others showed only one gully in the thalweg (several decimeters wide and deep). The retriangulation method presented in the Materials and methods section was used to create the pre-eroded surface. Because the method retriangulates the unaffected surface areas, it is only suitable for surfaces with low microrelief. Thus, aerial surveys and analyses of erosion quantity were conducted for 7 cornfields, where 33 rills were analyzed. The spread of the rills ranged from 10 to 580 m^2.

With the retriangulation method, a pre-erosion surface was created, and with the DEMs of difference method, the erosion depth was calculated at each grid point. As the differences in the DEMs are only located at the rill, all grid points should show negative values, which indicate erosion. Positive values indicate errors. For 97% of the investigated rills, the error was less than 4%, resulting in a standard deviation of 1.13%. One rill showed an error of approximately 30%. This rill was wide and shallow and contained vehicle lanes. Therefore, this rill was excluded from further analysis. Overall, no dependence of the error on the rill width, erosive slope length, or gradient was identified. Gully depth and bulk density were used to calculate the erosion volume of each rill. Information regarding the rills and catchment areas is presented in Table 2.

For each of the 32 analyzed rills, the mean rill width, LS factor for the rill catchment area, and precipitation volume for the rill catchment area were calculated. Comparisons of these factors with erosion quantity always showed an increase in each factor with an increase in erosion quantity.

The preliminary accuracy tests in this study (see Sect. Material and methods) showed that the erosion rill depth resulting from UAV recordings underestimates the existing rill depth. Thus, the erosion rates listed in Table 2 indicate the minimum of the expected erosion, which may be up to 20% higher.

Forecasting erosion using erosion models can be effective for developing measures to protect human lives, infrastructure, and valuable soils. In the following sections, two erosion models are used to calculate the erosion quantities of events recorded in this study: the well-known RUSLE2 as an empirical but easy-to-use model and E3D as a physically based erosion model that includes simplified flow accumulation processes.

Comparison using existing erosion models

Recent review articles (Andualem et al. 2023; Borelli et al. 2021) have shown that many erosion and sedimentation models are available worldwide. According to Batista et al. (2019), such models are not scarce. However, the knowledge and testing of transferability in different application cases and areas still require further research. For comparison with data from this study (Results Sect. Analysis of erosion quantity), the RUSLE2 and E3D models were applied to selected fields.

RUSLE2 model at the rill catchment area scale

To compare the RUSLE2 with the rill erosion data of this study, the RUSLE2 was applied to all rill catchment areas. For this analysis, the RUSLE2 was applied to a single event (R factor) for comparability reasons. The erosion quantity in this study represents only linear erosion and neglects sheet erosion owing to the quantification method (Methods Sect. Analysis of erosion quantity). Therefore, the RUSLE2 model was applied to calculate sheet and rill erosion (standard) and only to sheet erosion (interrill area). The difference between both values leads to the rill erosion share

Table 2 Results of erosion analyses

Reference		Max. erosion depth [m]	Erosion area [m^2]	Bulk density [kg/m^3]	Erosion volume [m^3]	Error [%]	Rill catchment area [ha]	Average slope (rill catchment area) [%]	Average length (rill catchment area) [m]	Erosion rate [t/ha]
Field no.	Area no.									
3	1	0.181	578.99	1,190	23.970	1.18	0.601	10.95	185	47.461
	2	0.148	184.18	1,190	5.174	1.99	0.341	10.97	160	18.056
	3	0.136	128.91	1,190	3.236	1.42	0.138	10.66	151	27.905
	4	0.097	24.45	1,190	0.519	0.96	0.071	9.22	66	8.699
	5	0.189	20.39	1,190	0.699	0.72	0.043	13.11	46	19.344
	6	0.152	23.04	1,190	0.791	0.76	0.093	10.95	121	10.121
	7	0.195	16.39	1,190	0.673	0.30	0.041	11.78	112	19.533
4	1	0.410	236.90	1,120	10.680	0.78	0.111	16.51	93	107.762
	2	0.185	239.87	1,120	7.302	1.68	0.126	16.13	100	64.907
	3	0.115	61.77	1,120	1.318	2.43	0.065	16.62	79	22.710
	4	0.129	63.60	1,120	1.289	1.86	0.088	16.20	90	16.405
	5	0.127	167.04	1,120	4.026	1.19	0.180	16.07	88	25.051
5	1	0.145	48.26	1,120	0.987	2.23	0.051	9.68	73	21.675
	2	0.810	9.39	1,120	0.141	3.55	0.147	11.64	73	1.074
6	1	0.130	96.01	1,200	2.563	2.30	0.218	10.91	118	14.108
	2	0.120	85.57	1,200	2.070	2.32	0.076	14.43	118	32.684
	3	0.124	113.2	1,200	2.675	3.55	0.165	12.68	135	19.455
	4	0.157	61.72	1,200	1.384	2.82	0.102	12.03	130	16.282
	5	0.118	35.32	1,200	0.938	1.60	0.051	14.84	73	22.071
	6	0.137	92.51	1,200	2.776	1.01	0.142	12.34	115	23.459
	7	0.124	17.96	1,200	0.509	0.79	0.056	13.84	94	10.907
7	1	0.089	32.75	1,420	0.416	3.61	0.028	14.28	31	21.097
	2	0.105	148.31	1,420	1.826	1.75	0.183	14.72	44	14.169
	3	0.156	80.94	1,420	1.552	0.64	0.050	13.60	59	44.077
	4	0.096	50.80	1,420	1.366	0.88	0.047	14.18	73	41.271
	5	0.109	79.97	1,420	2.214	1.04	0.061	12.55	108	51.539
	6	0.383	448.49	1,420	12.418	2.65	0.095	11.21	193	185.616
	7	0.175	267.89	1,420	10.481	1.10	0.411	11.47	245	36.212
	8	0.262	352.72	1,420	9.487	1.45	0.205	11.60	222	65.715
	9	0.116	99.93	1,420	2.503	1.12	0.241	11.84	235	14.748
	10	0.456	148.31	1,420	4.078	1.64	0.167	11.98	218	34.675
8	1	0.294	230.84	1,310	12.143	1.25	0.818	8.87	175	19.447

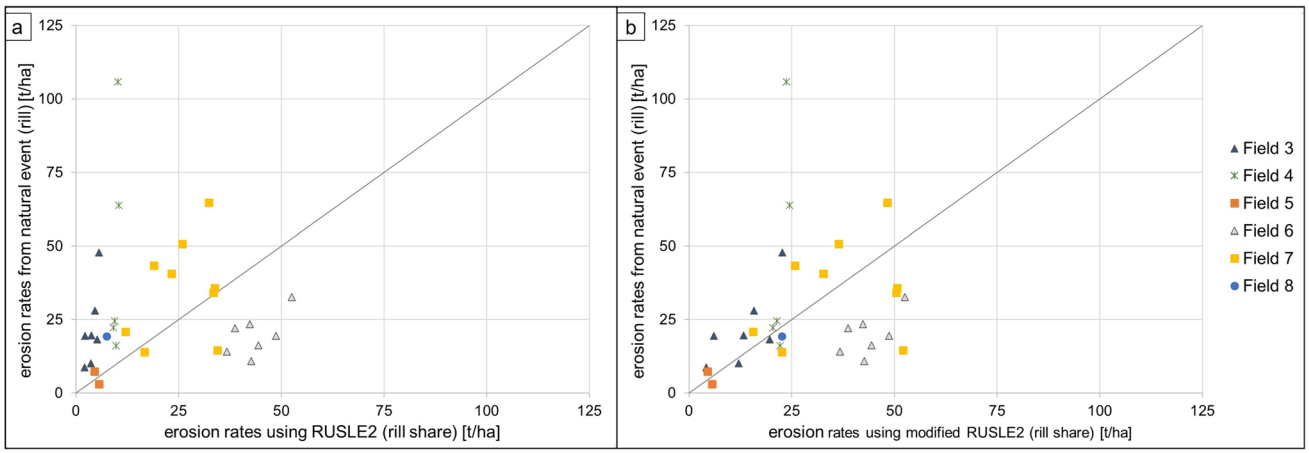

Fig. 3 Comparison of erosion rates from RUSLE2 rill erosion and erosion rates of linear erosion from the natural event (**a**), and the same graph with considered $(LS)^x$ in RUSLE2 equation for rill and interrill erosion (**b**). Here, x is 2 for Field 3, 1.5 for Field 4, 1 for Field 5, 1 for Field 6, 1.25 for Field 7, and 2 for Field 8. Each data point represents one rill. Different colors and forms of the points represent different fields. The graphs shown are limited to 125 t/ha, although one data point has a higher value in each graph. The gray line indicates the 1:1 line

of the RUSLE2 that was compared to the linear erosion of this study. The share of interrill and rill erosion is 15–42% and 58–85% respectively. In most cases, the share of rill erosion is around 80%.

The comparison of RUSLE2 rill erosion and the natural rill erosion is shown in Fig. 3a. Each symbol type represents one field and each data point one rill. It appears that the quality of RUSLE2 model values depends on the field. The erosion rate of the natural events was higher than the calculated rate using RUSLE2 for most rills. The percentage difference ranged from -75% to + 934% and the root mean square error (RMSE) is 38.26. An analysis of the rill characteristics shows that the rill expansion is decisive for the differences. The larger and more pronounced the rill, the higher the deviation compared to the RUSLE2. The higher the number and the smaller the rills, the lower the deviation. Hence, strong erosion leads to a higher error of RUSLE2, because larger rill systems are formed. For small rills, a correlation between the measured erosion and the erosion calculated using the RUSLE2 was apparent (Fig. 3a, Field 5) or RUSLE2 slightly overestimated the rill erosion (Fig. 3a, Field 6). This may have been because many small rills showed a similar amount of erosion or the erosion type recorded by the calibration data of the RUSLE2. In particular, the analysis showed that the recorded erosion that best matched the RUSLE2 erosion had a small LS factor compared to other data points. Therefore, LS is a significant factor in linear erosion. Erosion rates obtained using the RUSLE2 strongly underestimated the linear erosion quantities because linear erosion was not considered. This can be largely attributed to the test plots, where linear erosion tracks could not develop out of the surface flow. By considering the LS factor in the RUSLE2 to be a power, the erosion of the natural event approximated the RUSLE2 values better (Fig. 3b). With this modification, the percentage difference improves to a range from − 75% to + 345%. Here, a RMSE of 33.78 can be reached. Calculating the RUSLE2 with factor $(LS)^x$ does not represent an equation for linear erosion quantities. Rather, this demonstrates the strong influence of LS. However, the accuracy of this approach is limited as the USLE family models are not suitable for large rill and gully erosion.

In contrast, the K factor has a low influence on the amount of erosion calculated using the RUSLE2. For the rill catchment areas, the K factor ranged from 0.25 to 0.35. One outlier shows a value of 0.15. The minor influence of the factor becomes clear when K factors of 0.25–0.35 are replaced by a constant of 0.3. This modification alters the soil erosion using RUSLE2 by − 17% to + 17%.

The quantity of erosion depends on many different factors such as the volume and intensity of precipitation, slope length and gradient, soil, and vegetation cover. The combination of these factors depends on the site, crop and management choices of farmers, and natural events. Furthermore, the discharge of a flash flood, which accumulates at different velocities along the flow path, is significant for the dynamic forces on the soil and depends on specific surfaces. These surface conditions, including the gradient, often vary within the field, resulting in inaccurate considerations with empirical factors. Considering the flow accumulation and total flow, depending on the surface model, these restrictions are reduced. This approach was used in the erosion simulations using E3D software.

RUSLE2 and E3D at the rill catchment area scale

For this analysis, erosion quantities for single rills calculated using RUSLE2, E3D and results of this study were compared. The E3D and RUSLE2 models were applied to natural heavy precipitation events on three hillslopes recorded in this study. For E3D, the erosion quantity of the whole field, shown in Fig. 4, was calculated. For RUSLE2, the calculation for the rill catchment area remains unchanged compared to the previous Sect.. All erosion fields showed different rill types: Field 4: two large rills; Field 7: a large field with many small and shallow rills and a single large rill (without thalweg); Field 8: one rill in the thalweg.

The simulation results for the three fields using E3D are shown in Fig. 4. The sediment budget showed pink erosion and green sedimentation. Sheet erosion was clearly visible in all fields. In addition, more or less pronounced linear erosion tracks were observed. In particular, in Field 8, as shown in Fig. 4c, one rill in the thalweg of the field is visible. The position of the rill matched that of the natural event. Fields 4 and 7 show only small rills. In addition, these rills match the rills of recorded events. However, specifically in Field 7, many rills were not considered in the modeling results. For all visible rills, the erosion quantity of E3D was analyzed, and the RUSLE2 was applied to these rill catchments. The spatial distribution of the rills cannot be determined using the manual calculations of the RUSLE2. For the RUSLE 2, the values in Table 3 are in accordance with the values shown in Fig. 3a (change of the unit). The resulting erosion quantities are presented in Table 3.

The calculated erosion quantities of the natural events were always higher than those calculated using E3D or RUSLE2. Notably, the E3D reflects only a fraction of the recorded natural erosion, whereas the RUSLE2 simulates a higher share. However, it must be considered that E3D outputs the net erosion, while RUSLE2 outputs the gross erosion (without considering sedimentation). As the recording of the natural event in this study occurred after the event, the recorded natural erosion was also net erosion. Furthermore, Schmidt (1996) and von Werner (1995) claim that the E3D model calculate the detachment of linear erosion but no spatial or temporal initiation of rill erosion is available in the model. Thus, the application is limited to sheet erosion.

Conclusions

In the present study, 456 croplands were investigated over three years after heavy precipitation events in Saarland, Germany, and neighboring states. Analyses of field conditions showed that erosion occurred only in fields with bare soil or sparse vegetation. No erosion was detected in fields with a cover greater than 25%. Heavy precipitation-induced linear erosion was recorded using a UAV. The spatial distributions of the linear erosion tracks and erosion quantities were derived from aerial survey data. These data are appropriate for providing information on erosion quantities and rates based on heavy precipitation events and pronounced linear erosion at the hillslope scale. The measured erosion rates ranged from 1 to 185 t/ha.

Fig. 4 Simulation results of sediment budget obtained using E3D for Field 4 (**a**), Field 7 (**b**), and Field 8 (**c**)

Table 3 Linear erosion of rills in E3D and RUSLE2 models compared to calculated rill masses of this study

Field no.	Area no.	Rill type	Measurement natural event [t]	E3D [t]	Share of E3D in natural erosion [%]	RUSLE2 rill share [t]	Share of RUSLE2 (rill) in natural erosion [%]
4	1	One big rill (slight thalweg in DEM)	11.962	0.022	0.18	1.14	9.53
7	6	One big rill (no visible thalweg in DEM)	17.634	1.350	7.66	11.71	66.35
7	8	One big rill (slight thalweg in DEM)	13.472	0.565	4.19	7.81	57.97
8	1	One big rill (thalweg in DEM)	15.907	4.336	27.26	6.11	38.41

Comparisons of the empirically based erosion data of this study with the E3D and RUSLE2 model values indicate that the erosion of natural events does not fit the erosion quantities obtained using existing models (RUSLE2 and E3D). The model applications underestimated naturally occurring erosion tracks. The spatial distribution of the linear erosion tracks was considered in E3D for erosion that occurred in the thalweg. Overall, linear erosion was not sufficiently reproduced by the applied erosion models. In most existing models, the erosion data used for calibration are limited to test plots that do not reflect the LS factors of a hillslope. In this study, it was shown that LS was the most significant factor for the occurrence of linear erosion rather than sheet erosion. However, it was also shown that the parameter that considers soil properties (K factor) does not influence the erosion significantly. To correctly simulate the linear erosion caused by heavy precipitation, reliable calibration data based on these conditions must be considered. The data collected in this study are appropriate for this purpose. Further research is required to calibrate erosion models using data that is appropriate for heavy precipitation-induced erosion and, therefore, for linear erosion. Furthermore, existing models (e.g., E3D) consider overland flow using simplified approaches (hydrological modeling using GIS). However, the current state-of-the-art simulation of heavy precipitation events, such as pluvial flash floods, is a two-dimensional (2D) hydrodynamic numerical model. Using 2D models of flash floods to simulate erosion will improve our knowledge of the attacking forces of water, thereby increasing the accuracy of heavy precipitation-induced erosion modeling.

Acknowledgements The author thanks Prof. Dr. Alpaslan Yörük and Prof. Dr. Jochen Kubiniok for their support in all aspects. Thank you to Hydrotec Ingenieurgesellschaft für Wasser und Umwelt mbH for providing the FEWS system and thank you to the student assistants, who helped with the soil analyses and the analysis of the erosion quantity. Finally, the author thanks all parties who assisted with the UAV flights and the farmers who allowed investigation on their fields.

Author contributions The author confirms sole responsibility for the following: study conception and design, data collection, analysis and interpretation of results, and manuscript preparation.

Funding Open Access funding enabled and organized by Projekt DEAL. This study was supported by the Ministry of Environment, Saarland, Germany (Project SEROMO). The UAV was funded by the School of Architecture and Civil Engineering, University of Applied Sciences, Saarbrücken, Germany.

Data availability statement The datasets (DEMs and orthoimages) generated during this study are provided in a data repository (https://doi.org/10.6084/m9.figshare.24592338.v1).

Declarations

Conflict of interest The authors have no relevant financial or non-financial interests to disclose.

References

Agisoft LLC (n.d.). Software Agisoft Metashape Professional, Version 1.7.1, St. Petersburg

Aksoy H, Unal NE, Cokgor S, Gedikli A, Yoon J, Koca K, Inci SB, Eris E, Pak G (2013) Laboratory experiments of sediment transport from bare soil with a rill. Hydrol Sci J. https://doi.org/10.1080/02626667.2013.824085

Andualem TG, Hewa GA, Myers BR, Peters S, Boland J (2023) Erosion and sediment transport modeling: a systematic review. Land 12:1396. https://doi.org/10.3390/land12071396

Aquaveo. XMS Wiki. SMS:Mesh Node Triangulation. https://www.xmswiki.com/wiki/SMS:Mesh_Node_Triangulation. Accessed 10 Mar 2023

Aquaveo LLC (n.d.). Software SMS, Version 13.1.0, Provo

Armand R, Bockstaller C, Auzet A-V, Van Dijk P (2009) Runoff generation related to intra-field soil surface characteristics variability. Application to conservation tillage context. Soil Tillage Res 102:27–37. https://doi.org/10.1016/j.still.2008.07.009

Báčová M, Krása J, Devátý J, Kavka P (2019) A GIS method for volumetric assessments of erosion rills from digital surface models. Eur J Remote Sens 52(S1):96–107. https://doi.org/10.1080/22797254.2018.1543556

Batista PVG, Davies J, Silva MLN et al (2019) On the evaluation of soil erosion models: are we doing enough? Earth Sci Rev. https://doi.org/10.1016/j.earscirev.2019.102898

Boardman J, Favis-Mortlock D (eds) (1998) Modelling soil erosion by water. NATO ASI Subseries I, vol 55. https://doi.org/10.1007/978-3-642-58913-3

Borelli B, Alewell C, Alvarez P et al (2021) Soil erosion modelling: a global review and statistical analysis. Sci Total Environ 780:146494. https://doi.org/10.1016/j.scitotenv.2021.146494

Bruno C, Di Stefano C, Ferro V (2008) Field investigation on rilling in the experimental Sparacia area, South Italy. Earth Surf Process Landf 33:263–279. https://doi.org/10.1002/esp.1544

Bryan (ed) (1990) Soil erosion—experiments and models. Catena Supplement 17

Cândido BM, Quinton JN, James MR, Silva MLN, de Carvalho TS, de Lima W, Beniaich A, Eltner A (2020) High-resolution monitoring of diffuse (sheet or interrill) erosion using structure-from-motion. Geoderma 375:114477. https://doi.org/10.1016/j.geoderma.2020.114477

Carollo FG, Di Stefano C, Ferro V, Pampalone V (2015) Measuring rill erosion at plot scale by a drone-based technology. Hydrol Process 29:3802–3811. https://doi.org/10.1002/hyp.10479

Carollo FG, Serio MA, Pampalone V, Ferro V (2024) The unit plot of the Universal soil loss equation (USLE): myth or reality? J Hydrol 632:130880. https://doi.org/10.1016/j.jhydrol.2024.130880

D'Oleire-Oltmanns S, Marzolff I, Peter KD, Ries JB (2012) Unmanned aerial vehicle (UAV) for monitoring soil erosion in Morocco. Remote Sens 4(11):3390–3416. https://doi.org/10.3390/rs4113390

Deltares (n.d.). Software Delft-FEWS, Version 2019.02, Delft

Di Stefano C, Ferro V, Palmeri V, Pampalone V (2017) Measuring rill erosion using structure from motion: a plot experiment. CATENA 156:383–392. https://doi.org/10.1016/j.catena.2017.04.023

Di Stefano C, Palmeri V, Pampalone V (2019) An automatic approach for rill network extraction to measure rill erosion by terrestrial and low-cost unmanned aerial vehicle photogrammetry. Hydrol Process 33:1883–1895. https://doi.org/10.1002/hyp.13444

DIN Deutsches Institut für Normung (2017a) DIN 19708:2017-08, Bodenbeschaffenheit – Ermittlung der Erosionsgefährdung von Böden durch Wasser mit Hilfe der ABAG [Soil quality—predicting soil erosion by water by means of ABAG]. Beuth, Berlin

DIN Deutsches Institut für Normung (2017b) DIN EN ISO 17892-4:2017-04, Geotechnische Erkundung und Untersuchung - Laborversuche an Bodenproben - Teil 4: Bestimmung der Korngrößenverteilung [Geotechnical investigation and testing—laboratory testing of soil—part 4: determination of particle size distribution]. Beuth, Berlin

DIN Deutsches Institut für Normung (2020) DIN 18125-2:2020-11, Baugrund, Untersuchung von Bodenproben - Bestimmung der Dichte des Bodens - Teil 2: Feldversuche [Soil, investigation and testing—determination of density of soil—part 2: field tests]. Beuth, Berlin

DWA Deutsche Vereinigung für Wasserwirtschaft Abwasser und Abfall e. V (2020) DWA-Regelwerk, Merkblatt DWA-M 921. Bodenerosion durch Wasser – Kartieranleitung zur Erfassung aktueller Erosionsformen [Soil erosion by water—Mapping guideline to record current erosion forms], Entwurf. Druckhaus köthen GmbH & Co KG. Hennef

Deutscher Wetterdienst (DWD). Wetter- und Klimalexikon. Starkregen. https://www.dwd.de/DE/service/lexikon/Functions/glossar.html?nn=103346&lv2=102248&lv3=102572. Accessed 14 Mar 2023

Deutscher Wetterdienst (DWD) (2004) Projekt RADOLAN, Routineverfahren zur Online-Aneichung der Radarniederschlagsdaten mit Hilfe von automatischen Bodenniederschlagsstationen (Ombrometer). Zusammenfassender Abschlussbericht für die Projektlaufzeit von 1997 bis 2004. https://www.dwd.de/DE/leistungen/radolan/radolan_info/abschlussbericht_pdf.pdf?__blob=publicationFile&v=2. Accessed 10 Mar 2023

Deutscher Wetterdienst (DWD) (2004) RADOLAN: radar online adjustment, radar based quantitative precipitation estimation products, poster. https://www.google.com/url?sa=t&rct=j&q=&esrc=s&source=web&cd=&ved=2ahUKEwjK_duoodH9AhXaSPEDHe6VCRQQFnoECBcQAQ&url=https%3A%2F%2Fwww.dwd.de%2FDE%2Fleistungen%2Fradolan%2Fradolan_info%2Fradolan_poster_201711_en_pdf.pdf%3F__blob%3DpublicationFile%26v%3D2&usg=AOvVaw2xtcS2EXfUWE9LQtc7RuPV. Accessed 10 Mar 2023

Eltner A, Baumgart P, Maas H-G, Faust D (2015) Multi-temporal UAV data for automatic measurement of rill and interrill erosion on loess soil. Earth Surf Process Landf 40:741–755. https://doi.org/10.1002/esp.3673

GeoGnostics (n.d.). Software EROSION-3D, Version 3.3.2.3.32, Berlin

Giménez R, Marzolff I, Campo MA, Seeger M, Ries JB, Casalí J, Álvarez-Mozos J (2009) Accuracy of high-resolution photogrammetric measurements of gullies with contrasting morphology. Earth Surf Process Landf 34:1915–1926. https://doi.org/10.1002/esp.1868

IPCC (2021) Summary for Policymakers. In: Climate change 2021: the physical science basis. Contribution of Working Group I to the Sixth Assessment Report of the Intergovernmental Panel on Climate Change; Masson-Delmotte, V., Zhai, P., Pirani, A., Connors, S.L., Péan, C., Berger, S., Caud, N., Chen, Y., Goldfarb, L., Gomis, M.I., et al., Eds.; Cambridge University Press, Cambridge, New York, pp 3–32. https://doi.org/10.1017/9781009157896.001

Kou P, Xu Q, Yunus AP, Ju Y, Guo C, Wang C, Zhao K (2020) Multitemporal UAV data for assessing rapid rill erosion in typical gully heads on the largest tableland of the Loess Plateau, China. Bull Eng Geol Environ 79:1861–1877. https://doi.org/10.1007/s10064-019-01631-x

Laflen JM, Lane LJ, Foster GR (1991) WEPP: a new generation of erosion prediction technology. J Soil Water Conserv 46:34–38

LVGL Landesamt für Vermessung, Geoinformation und Landentwicklung (2019) Digitale Geländemodelle [Digital elevation models]. https://www.saarland.de/lvgl/DE/themen-aufgaben/themen/geotopographie/digitalegelaendemodelle/digitalegelaendemodelle.html. Accessed 12 Jan 2022

LVGL Landesamt für Vermessung; Geoinformation und Landentwicklung (n.d.) Geoportal Saarland, ALKIS Bodenschätzung (Ressourcenidentifikator: 41583)

Malinowski R, Heckrath G, Rybicki M, Eltner A (2022) Mapping rill soil erosion in agricultural fields with UAV-borne remote sensing data. Earth Surf Process Landf. https://doi.org/10.1002/esp.5505

Michael A (2000) Anwendung des physikalisch begründeten Erosionsprognosemodells EROSION 2D/3D—Empirische Ansätze zur Ableitung der Modellparameter. Doctoral thesis

Michael A, Schmidt J, Schmidt WA (1996) Erosion 2D/3D. Ein computermodell zur simulation der bodenerosion durch wasser. Parameterkatalog sachsen. Anwendungen

Morgan RPC, Quinton JN, Smith RE, Govers G, Poesen JWA, Auerswald K, Chisci G, Torri D, Styczen ME (1998) The European soil erosion model (EUROSEM): a process-based approach for predicting soil loss from fields and small catchments. Earth Surf Process Landf 23:527–544. https://doi.org/10.1002/(SICI)1096-9837(199806)23:6%3c527::AID-ESP868%3e3.0.CO;2-5

Morgan RPC, Nearing MA (eds) (2011) Handbook of erosion modelling. Blackwell Publishing Ltd. https://doi.org/10.1002/9781444328455

Parkin GW, Gardner WH, Auerswald K (2008) Water erosion. In: Chesworth W (eds) Encyclopedia of soil science. Encyclopedia of earth sciences series. Springer, Dordrecht. https://doi.org/10.1007/978-1-4020-3995-9_625

Peter KD, d'Oleire-Oltmanns S, Ries JB, Marzolff I, Aït Hssaine A (2014) Soil erosion in gully catchments affected by land-levelling measures in the Souss Basin, Morocco, analysed by rainfall simulation and UAV remote sensing data. CATENA 113:24–40. https://doi.org/10.1016/j.catena.2013.09.004

Pineux N, Lisein J, Swerts G, Bielders CL, Lejeune P, Colinet G, Degré A (2017) Can DEM time series produced by UAV be used to quantify diffuse erosion in an agricultural watershed? Geomorphology 280:122–136. https://doi.org/10.1016/j.geomorph.2016.12.003

Polyakov V, Stone J, Holifield Collins C, Nearing MA, Paige G, Buono J, Gomez-Pond R-L (2018) Rainfall simulation experiments in the southwestern USA using the Walnut Gulch Rainfall Simulator. Earth Syst Sci Data 10:19–26. https://doi.org/10.5194/essd-10-19-2018

Römkens MJM, Helming K, Prasad SN (2001) Soil erosion under different rainfall intensities, surface roughness, and soil water regimes. CATENA 46:103–123. https://doi.org/10.1016/S0341-8162(01)00161-8

Schmidt J (1984) Experimentelle Untersuchungen und Modellvorstellungen zur Bodenerosion durch Wasser. Mitteilg Dtsch Bodenkdl Gesellsch 39:139–144

Schmidt J (1988) Wasserhaushalt und Feststofftransport an geneigten, landwirtschaftlich bearbeiteten Nutzflächen. Dissertation, FU Berlin

Schmidt J (1996) Entwicklung und Anwendung eines physikalisch begründeten Simulationsmodells für die Erosion geneigter landwirtschaftlicher Nutzflächen. Berliner Geogr. Abb., Heft 61, Berlin, pp 1–148

Schwertmann U, Vogl W, Kainz M (1987) Bodenerosion durch Wasser. Vorhersage des Abtrags und Bewertung von Gegenmaßnahmen. 2. Auflage. Stuttgart

Tackmann R (2010) Analysis of rill erosion in cohesive soils. Doctoral thesis

USDA (2008) Draft user's reference guide. Revised Universal Soil Loss Equation Version 2 (RUSLE2). USDA-Agricultural Research Service. Washington, D.C. https://www.ars.usda.gov/southeast-area/oxford-ms/national-sedimentation-laboratory/watershed-physical-processes-research/research/rusle2/revised-universal-soil-loss-equation-2-rusle2-documentation/

USDA (2013) Science Documentation: Revised Universal Soil Loss Equation Version 2 (RUSLE2) (for the model with release date of May 20, 2008). USDA-Agricultural Research Service. Washington, D.C. https://www.ars.usda.gov/southeast-area/oxford-ms/national-sedimentation-laboratory/watershed-physical-processes-research/research/rusle2/revised-universal-soil-loss-equation-2-rusle2-documentation/

Winterrath T, Brendel C, Hafer M, Junghänel T, Klameth A, Lengfeld K, Walawender E, Weigl E, Becker A (2018) RADKLIM Version 2017.002: reprocessed quasi gauge-adjusted radar data, 5-minute precipitation sums (YW). https://doi.org/10.5676/DWD/RADKLIM_YW_V2017.002

Wirtz S, Seeger M, Ries JB (2010) The rill experiment as a method to approach a quantification of rill erosion process activity. Z Geomorphol 54(1):47–64. https://doi.org/10.1127/0372-8854/2010/0054-0004

Wirtz S, Seeger M, Ries JB (2012) Field experiments for understanding and quantification of rill erosion processes. CATENA 91:21–34. https://doi.org/10.1016/j.catena.2010.12.002

Wischmeier WH, Smith DD (1978) Predicting rainfall erosion losses. Agric Handb 537:285–291. https://doi.org/10.1029/TR039i002p00285

Zhang L, Liu X, Song Y, Li J, Cai C, Zhao X, Li Z (2021) Characterization of surface runoff pathways and erosion using hydrological attributes under simulated rainfall. Front Earth Sci 2021(9):683473. https://doi.org/10.3389/feart.2021.683473